

Time-Domain Mixed-Signal Vector-by-Matrix Multiplier Exploiting 1T-1R Array

Shubham Sahay, *Member, IEEE*, Mohammad Bavandpour, Mohammad Reza Mahmoodi, and Dmitri Strukov, *Senior Member, IEEE*

Abstract— The emerging mobile devices in this era of internet-of-things (IoT) require a dedicated processor to enable computationally intensive applications such as neuromorphic computing and signal processing. Vector-by-matrix multiplication (VMM) is the most prominent operation in these applications. Therefore, compact and power-efficient VMM blocks are required to perform resource-intensive computations. To this end, in this work, for the first time, we propose a time-domain mixed-signal VMM exploiting a modified configuration of 1 MOSFET-1 RRAM (1T-1R) array which overcomes the energy inefficiency of the current-mode VMM approaches based on RRAMs. In the proposed approach, the inputs and outputs are encoded in digital domain as duration of the pulses while the weights are realized as programmable current sinks utilising the modified 1T-1R blocks in the analog domain. We perform a rigorous analysis of the different factors which may degrade the compute precision of the proposed approach. We show that there exists a trade-off between the compute precision, dynamic range and the area and energy efficiency of the proposed VMM implementation. Therefore, we also provide the necessary design guidelines for optimising the performance. The preliminary results show that an effective compute precision of 6-bits is achievable owing to the inherent compensation effect. A 4-bit 200×200 VMM utilising the proposed approach exhibits a significantly high energy efficiency of ~1.5 POps/J and a throughput of 2.5 TOps/s while considering the contribution due to the input/output (I/O) circuitry.

Index Terms— Vector-by-matrix multiplication, 1T-1R array, Time-domain encoding, mixed-signal VMM.

I. INTRODUCTION

The widespread use of computationally intensive applications such as deep neural networks (DNNs)/recurrent neural networks (RNNs), real-time signal processing and optimization algorithms in this era of internet-of-things (IoT) necessitates the development of dedicated processing blocks within the mobile devices since the traditional digital processors are extremely energy inefficient while handling high-dimensional data from operations such as object/speech recognition, image processing, probabilistic inference, etc. [1]-[2]. The vector-by-matrix multiplication (VMM) forms the most integral part (and often bottleneck) of these computationally intensive systems. Therefore, the development of a compact, highly precise and energy efficient VMM engine is highly essential [3]-[16].

The analog-domain VMM implementations are more compact and energy-efficient as compared to the digital counterparts for computational tasks such as inference, classification, recognition, etc. which are robust to low resolution (reduced precision) VMM operations and can be trained effectively to handle hardware imperfections without compromising with the accuracy [3], [6]-[10]. Recently, VMMs based on emerging non-volatile memories, RRAMs in particular, have attracted considerable attention since the VMM operation is simplified as current accumulation through programmable resistances in analog domain [5]-[6], [10]. However, the current-mode VMM implementations based on RRAM require high current levels [6], [16] and bulky trans-impedance amplifiers at each column of the cross-bar [6] degrading its energy and area efficiency. Moreover, the compute precision is also limited and may be improved only at the cost of an increased area for complex peripheral circuitry to implement sophisticated tuning algorithms or complex mapping techniques [6].

Recently, time-domain VMMs [4], [9]-[15] exploiting flash memory [15], post-synaptic pulse (PSP) emulators [11], and SRAM (binary) output [13] as programmable weights have been proposed. Moreover, the energy efficiency of the RRAM based VMM approaches could be significantly improved if a time-domain switched capacitor based approach [8] is followed as opposed to the power-hungry current-mode approach. To this end, in this work, for the first time, we propose a time-domain mixed-signal VMM exploiting a modified 1MOSFET-1RRAM (1T-1R) array. In the proposed VMM approach, the weights are realized as programmable current sinks via tuning the RRAM conductance state in the modified 1T-1R blocks in the analog domain while the inputs and outputs are encoded as pulse durations in the digital domain. Contrary to the conventional 1T-1R blocks, where RRAM is connected to the drain of the MOSFET, the RRAM is attached to the source in this approach which leads to a self-compensation effect and significantly improves the compute precision. A rigorous analysis of the different non-ideal factors affecting the compute precision of the proposed VMM indicate that channel length modulation (CLM) and drain-induced barrier lowering (DIBL) are the dominant mechanisms degrading the compute precision. Furthermore, we also show that there exists a trade-off between

The authors are with the California Nano Systems Institute (CNSI) and also with the Department of Electrical and Computer Engineering, University of California, Santa Barbara, California, 93106, U.S.A.

(e-mail: shubhamsahay@ucsb.edu)

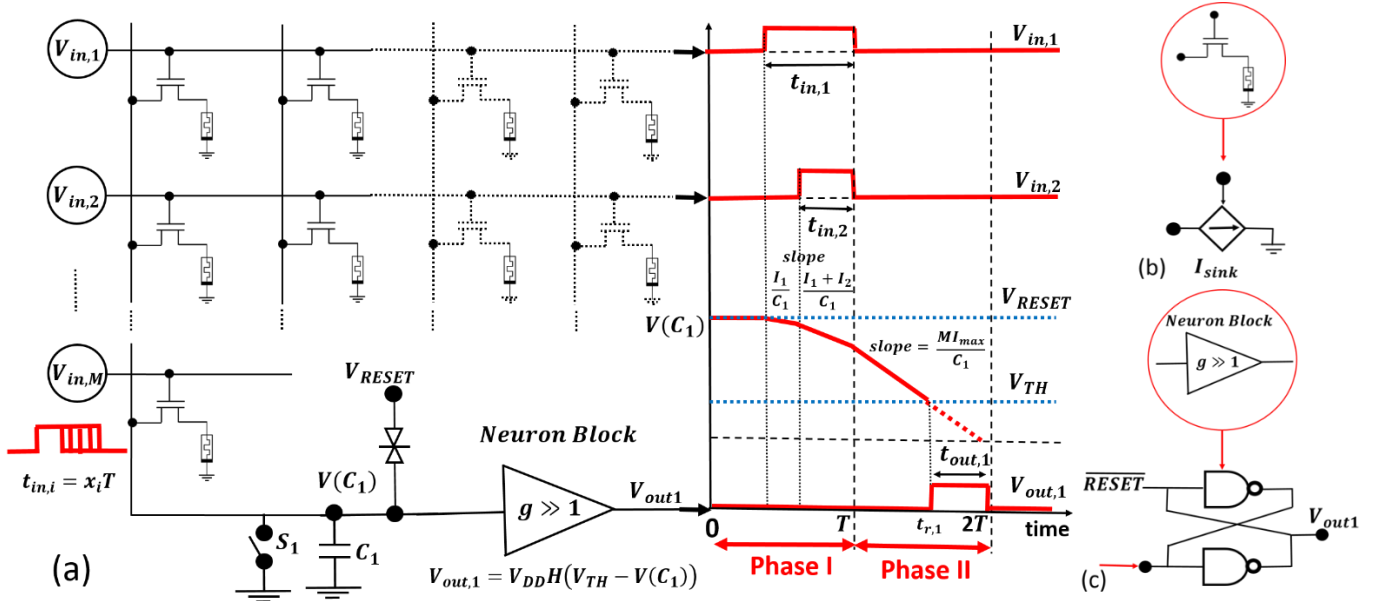


Fig.1 Schematic view of (a) the VMM circuit utilizing 1T-1R array and the timing diagram of the inputs, outputs and the voltage across the load capacitor, (b) the modified 1T-1R block which acts as a programmable current sink and (c) the peripheral circuit within the neuron block implementing the Heaviside function.

the compute precision, dynamic range and the area and energy dissipation in this implementation. Therefore, we also provide the necessary design guidelines for optimizing the performance of the proposed architecture. The preliminary results show that an effective precision of 6-bits may be obtained utilizing this approach with an energy efficiency of ~ 498.5 Tops/J and a throughput of 1.9 Tops/s for a 200×200 VMM.

The paper is organized as follows: the proposed VMM approach is discussed in section II. The load-line characteristics of the modified 1T-1R block, the different factors which may affect the performance of the proposed approach are discussed in section III. The design guidelines for optimizing the performance of the proposed 1T-1R VMM are discussed in section IV and the area, energy and throughput estimates are discussed in section V. The conclusions are drawn in section VI.

II. PROPOSED VMM APPROACH

A generalized $M \times N$ VMM operation may be represented as:

$$y_j = \frac{1}{M} \sum_{i=1}^M w_{ij} x_i, \quad j = 1, 2, \dots, N \quad (i)$$

where the inputs x_i , outputs y_j and weights w_{ij} are normalized such that $(x_i, y_j, w_{ij}) \in [0, 1]$. The proposed time-domain VMM approach exploiting the modified 1T-1R array is shown in Fig. 1. In the time-domain VMM [9]-[15], the inputs are encoded as duration of the digital pulses such that:

$$t_{in,i} = x_i T \quad (ii)$$

where T is the time window for the VMM operation. In the proposed approach, the modified 1T-1R block acts as a programmable current sink as shown in Fig. 1(b) and the digital inputs applied to the gate of the MOSFETs ($V_{in,i}$) enable the i^{th} current sink for a duration $t_{in,i}$. It may be noted that unlike conventional 1T-1R arrays where the RRAMs are connected to the drain of the MOSFETs, in this approach, the RRAMs are connected to the source of the MOSFETs to dissuade the non-

idealities such as channel length modulation (CLM) and drain induced barrier lowering (DIBL) owing to the self-compensation effect as discussed in section III.C. The weights ($w_{ij} \in [0, 1]$) are mapped to the currents ($I_{ij} \in [I_{min}, I_{max}]$) through the programmable current sink as:

$$I_{ij} = I_{min} + w_{ij}(I_{max} - I_{min}) \quad (iii)$$

Each column of the programmable current sinks is connected to a load capacitor C_j . A threshold (neuron) circuit proposed in [14] with a transfer function given as:

$$V_{outj} = V_{DD}H(V_{TH} - V(C_j)) \quad (iv)$$

where $H()$ is the Heaviside function encodes the voltage on load capacitor C_j into output digital pulse duration.

The entire VMM operation is completed in two cycles (phase-I and phase-II) of duration T each. The load capacitor C_j is initially pre-charged to a voltage V_{RESET} at the beginning of phase-I ($t = 0$). The inputs are activated only in phase-I (integration phase) and the current sinks start discharging C_j . At the end of phase-I ($t = T$), the voltage across the load capacitor $V(C_j)$ reduces by $\Delta V(C_j)$ where:

$$\Delta V(C_j)_{t=T} = \frac{1}{C_j} \sum_{i=1}^M I_{ij} t_{in,i} \quad (v)$$

Using the expression for I_{ij} from equation (iii) in equation (v), we get:

$$\Delta V(C_j)_{t=T} = \frac{T(I_{max} - I_{min})}{C_j} \sum_{i=1}^M w_{ij} x_{in,i} + \frac{TI_{min}}{C_j} \sum_{i=1}^M x_{in,i} \quad (vi)$$

As evident from equation (vi), the change in the voltage across the load capacitor at the end of phase I is mapped to a linear expression of the weighted sum in this scheme. To ensure that this voltage variation across the load capacitor is limited to a targeted operation regime, i.e. $V(C_j)_{t=T} \in [V_{RESET}, V_{TH}]$, the load capacitor C_j must be designed such that:

$$C_j = \frac{MI_{max}T}{V_{RESET} - V_{TH}} \quad (vii)$$

In phase-II (evaluation phase), all the inputs are inactivated and the load capacitor is discharged through a constant current MI_{max} . This discharging current may be generated either via a current mirror or by adding a similar 1T-1R array at the load capacitor with all the inputs activated for the entire duration T during phase-II and the current sinks programmed to I_{max} . In this work, we have followed the latter approach to implement the constant current source during phase-II. The neuron circuit generates an output pulse when the voltage on the load capacitor reaches the threshold voltage i.e. ($V(C_j) = V_{TH}$). The time instance ($t_{r,j}$) at which $V(C_j) = V_{TH}$ can be given as:

$$t_{r,j} = T - t_{out,j} = T \left[1 - \frac{\sum_{i=1}^M I_{ij} t_{in,i}}{MI_{max}T} \right] \quad (\text{viii})$$

The output pulse duration ($t_{out,j}$) can be simply obtained by using equations (i) and (iii) in equation (viii) as:

$$t_{out,j} = ay_jT + b \quad (\text{ix})$$

where,

$$a = \frac{(I_{max} - I_{min})}{I_{max}}, \quad b = \frac{I_{min}}{MI_{max}} \sum_{i=1}^M x_{in,i}. \quad (\text{x})$$

Equation (ix) clearly indicates that the output result obtained using the proposed scheme is different from the targeted ideal output result ($t_{out,j} = y_jT$) due to the non-zero minimum current (I_{min}) of the 1T-1R cells which lead to the undesirable multiplicative coefficient (a) and the input-dependent additive coefficient (b).

However, it may be noted that the input-dependent additive coefficient (b) can be cancelled out by utilizing the differential scheme. In the differential implementation, each weight is realized utilizing two sub-weights w_{ij}^+ and w_{ij}^- such that

$$w_{ij} = w_{ij}^+ - w_{ij}^- \quad (\text{xi})$$

and two sub-neurons are dedicated to calculate the dot product of inputs and each sub-weight vector as $t_{out,j}^+$ and $t_{out,j}^-$ as:

$$t_{out,j}^+ = \frac{a}{M} \sum_{i=1}^M w_{ij}^+ x_i + b \quad (\text{xii})$$

$$t_{out,j}^- = \frac{a}{M} \sum_{i=1}^M w_{ij}^- x_i + b \quad (\text{xiii})$$

A simple logic circuitry is then employed to generate the final differential output pulse as:

$$t_{out,j} = t_{out,j}^+ - t_{out,j}^- \quad (\text{xiv})$$

On the other hand, the multiplicative coefficient (a) leads to a reduction in the output time window. This shrinkage can be compensated by either lowering the constant current during the evaluation phase (which extends the time window for phase II), or increasing the output time-to-digital convertor (TDC) counter frequency.

III. 1T-1R VMM DESIGN GUIDELINES

The performance of the proposed 1T-1R VMM was evaluated at the 55-nm technology node using PDK from Global Foundries in HSPICE (version N-2017.12[17]). MOSFETs with minimum width (120 nm) were used for all the analysis. Furthermore, a rather simplistic compact model was used for RRAM with the current-voltage relationship expressed as:

$$I_{mem} = g_0 \sinh(\beta V_{mem}) \quad (\text{xv})$$

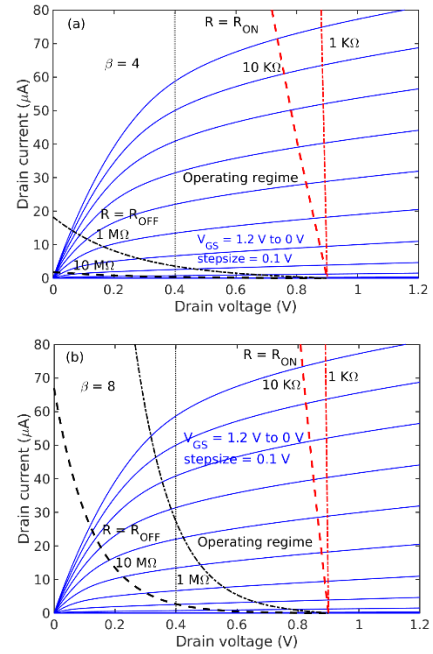


Fig. 2 The load line characteristics of the modified 1T-1R block for RRAMs with different non-linearity factor (a) $\beta = 4$ and (b) $\beta = 8$.

where g_0 is the conductance in the initial state and β is the non-linearity factor [18]. A maximum ON-state conductance ($g_0 = g_{max}$) of 0.1 mS ($R_{ON} = 10 \text{ K}\Omega$) and a minimum OFF-state conductance ($g_0 = g_{min}$) of 0.1 μS ($R_{OFF} = 10 \text{ M}\Omega$) were considered for RRAM similar to [6]. Furthermore, a maximum permissible read voltage of 0.5 V without disturbing the programmed state of RRAM was assumed. Under these assumptions, we evaluated the potential of the proposed 1T-1R time-domain VMM under different operating conditions and different parameters for the RRAM. In the subsequent sections, we discuss the operating conditions and provide the necessary design guidelines to extract the optimum performance from the proposed VMM architecture. It may be noted that the optimal conditions also differ with the input constraints such as VMM size, input voltage, time window, dynamic range ($DR = I_{max} - I_{min}$), targeted precision, etc.

A. Load-line characteristics

The load-line characteristics of the modified 1T-1R block shown in Fig. 1(b) (MOSFET with minimum gate length, $L_g = 60 \text{ nm}$) is shown in Fig. 2 for different non-linearity factors (β). The reset voltage V_{RESET} was chosen as 0.9 V to reduce the error induced due to non-idealities such as CLM and DIBL (as discussed in section III.C). From Fig. 2, we observe that increasing the non-linearity factor of the RRAM results in a reduction of the operating range of drain voltage for low gate voltages ($< 0.6 \text{ V}$). A reduced operating range of drain voltage leads to a lower dynamic range of current values which may be obtained from the modified 1T-1R block via tuning the conductance state of the RRAM (as can also be observed from Table I). Also, the ON-state to OFF-state conductance ratio of the RRAM should be high to obtain an appreciable DR .

Moreover, the operating range of drain voltages is also degraded when a RRAM with lower ON-state conductance or a higher OFF-state conductance is used as shown in Fig. 2. Furthermore, unlike the current-mode VMM approach based on RRAM where the accumulated current depends exclusively on the conductance state of the RRAMs, the current from the modified 1T-1R block depends both on the conductance state of the RRAM and the channel conductance of the MOSFET (which depends on the input voltage). Therefore, even if the ON-state conductance of RRAM increases by tenfold, as shown in Fig. 2, the drain current increases only slightly (< 2 times) and does not degrade the energy efficiency of the proposed VMM approach considerably as opposed to the current-mode VMM where the accumulated current would increase by a decade and limit the energy efficiency. However, the DR also increases for lower ON-state resistances of the RRAM in 1T-1R configuration.

B. Precision

The effective weight precision (i.e. programmability of the current sinks) depends on the accuracy of tuning the conductance states of RRAM and degrades due to the drift in the analog conductance state with cycling and temperature and the inherent intrinsic noise such as RTN exhibited by the RRAM. Previous works have already shown an effective weight precision greater than 7-bits based on a simple tuning algorithm [19]. The weight precision may be further improved by oxide material engineering or by utilizing more efficient tuning algorithms.

As discussed in [15], the compute error (or output error, e_{outj}) may be decoupled from the weight error and defined separately as the maximum difference between the theoretically calculated output time period considering ideal current sinks (t_{outj}^{cal}) and the output time period obtained via transient simulation of the entire VMM circuit (t_{outj}^{sim}), spanning over the entire sample space of the weights and inputs i.e.

$$e_{outj} = \max_{t_{outj}} \frac{|t_{outj}^{cal} - t_{outj}^{sim}|}{T} \quad (xvi)$$

The compute precision (P_{outj}) can then be defined as:

$$P_{outj} = -\log_2 e_{outj} - 1 \quad (xvii)$$

Considering the efficacy of the differential scheme in cancelling the impact of the input-dependent additive coefficient (b) as discussed in section II and improving the noise immunity and enhancing the output precision while enabling inclusion of bipolar weights [8], two adjacent columns of the 1T-1R array were tuned for implementing the positive and negative weight components of the bipolar weight matrix. Furthermore, the adjacent neuron circuits were used to calculate the positive ($V_{outj} = t_{out,j}^+$) and negative ($V_{out(j+1)} = t_{out,j}^-$) component of output in this differential implementation. Moreover, the final output was obtained as the time difference between the rising edge of the neuron circuits used for obtaining the positive (V_{outj}) and negative ($V_{out(j+1)}$) component of the output. This rectified linear (ReLU) operation may be

implemented utilizing a digital gate for $V_{finalj} = V_{outj} \cdot \overline{V_{out(j+1)}}$.

C. Non-ideal factors

The compute precision is degraded by several factors which tend to deviate the current sink from providing a constant current. While CLM leads to a linear dependence of the MOSFET's drain current on the drain voltage and restricts their action as constant current sink, the DIBL effect induces threshold voltage shift which further increases the variation in the drain current with the drain voltage. Therefore, in addition to the input voltage (V_{GS}), the current through the programmable 1T-1R current sink also depends on the drain voltage i.e. the output voltage at the load capacitor.

To minimize this dependency of the current sink on the output voltage, we modified the conventional 1T-1R array architecture. While the RRAM is connected to the drain terminal of the MOSFET in the conventional 1T-1R array, one terminal of RRAM is connected to the source of the MOSFET and the other terminal is grounded in this implementation as shown in Fig. 1(b). An increase in the drain voltage in the modified 1T-1R configuration with RRAM connected to the source leads to an enhanced current flowing through the RRAM. This results in a larger voltage drop across the RRAM. The increased voltage drop across the RRAM effectively boosts the source potential leading to a reduction in the effective gate to source voltage (V_{GS}) which in turn suppresses the increment in the drain current. Therefore, the increment in the drain current due to application of a larger drain voltage is compensated by a reduction in the effective gate overdrive voltage in the modified 1T-1R array. This inherent compensation effect leads to a diminished dependency of the current through the programmable current sink on the output voltage at the load capacitor.

The error due to CLM and DIBL can be defined as:

$$e_{CLM/DIBL} = 1 - \frac{I(V-\Delta V)}{I(V)} \quad (xviii)$$

where ΔV is chosen as 1mV to estimate the local error contours with accuracy. We performed a rigorous analysis of the CLM and DIBL error for different gate (input) voltages and non-ideality factors within the operating regime of the modified 1T-1R configuration. The error contour plots for different input voltages and non-linearity factors of RRAM are shown in Fig. 3. For all the input voltages, we found that the programmable current sink is relatively independent of the drain voltage (i.e. the CLM/DIBL error is low) for high drain voltages. Therefore, we selected a high reset voltage, $V_{RESET} = 0.9$ V and designed the neuron circuit to have a threshold voltage $V_{TH} = 0.7$ V to ensure a non-disturbing maximum voltage swing of 0.2 V across the RRAM. Furthermore, we also observe from Fig. 3 that the DIBL/CLM error increases as we reduce the input voltage and operate with a smaller maximum current (I_{max}) to limit the load capacitance (see equation (vii)). Moreover, the increased non-linearity factor of the RRAM leads to a significant reduction in the dynamic range as shown in Fig. 3(b).

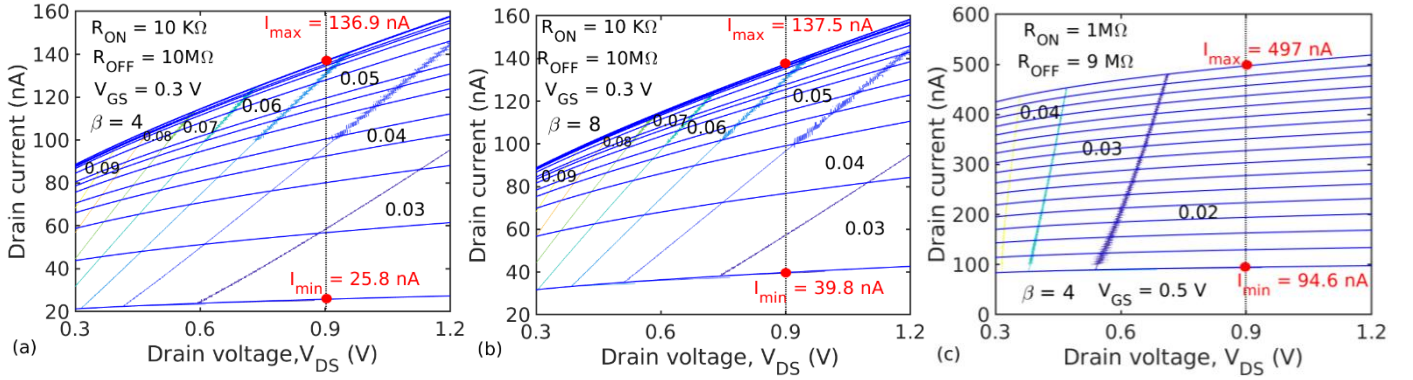


Fig. 3 The error contour plot due to the DIBL and CLM effect for different input voltages and non-ideality factors: (a) $V_{GS} = 0.3$, $\beta = 4$ and (b) $V_{GS} = 0.3$, $\beta = 8$ and (c) $V_{GS} = 0.5$ and $\beta = 4$ for MOSFETs with $L_g = 120$ nm.

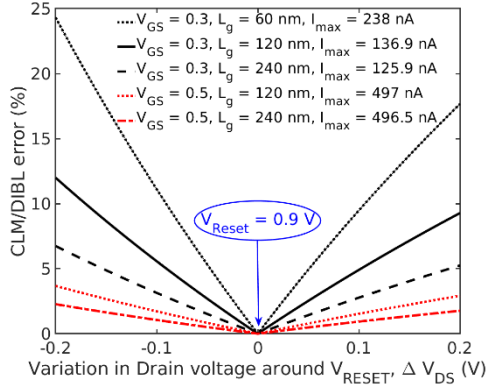


Fig. 4 The total error due to the DIBL and CLM effect for different input voltages and gate lengths (L_g) of the MOSFET with non-ideality factor, $\beta = 4$.

Since the DIBL and CLM effects are extremely sensitive to the gate length (L_g) of the MOSFETs, we also performed a thorough investigation of the CLM/DIBL error for 1T-1R blocks with MOSFETs of different gate lengths biased at different input voltages as shown in Fig. 4. We found that despite the self-compensation effect, the CLM/DIBL error is significantly high in the MOSFETs with minimum gate length ($L_g = 60$ nm) and reduces drastically by ~ 5 times when the gate length is quadrupled to $L_g = 240$ nm for the same input voltage. Moreover, the CLM/DIBL error can be further reduced while obtaining a higher DR by increasing the input voltage at the cost of an increased capacitor area and energy owing to larger I_{max} . Therefore, there exists a trade-off between area and energy efficiency, the dynamic range and the compute error in the proposed approach.

Apart from the error induced due to CLM and DIBL, the capacitive coupling between the load capacitor and the gate-drain capacitance of the MOSFET could be another possible source of charge disturbance. However, in the proposed architecture, the load capacitor is large compared to the gate-drain capacitance of the minimum sized MOSFETs owing to the higher maximum current I_{max} . This diminishes the charge disturbance due to capacitive coupling.

IV. DESIGN SPACE EXPLORATION

We also performed a rigorous analysis to explore the design space for optimizing the performance of the proposed VMM architecture. The input voltage (V_{GS}) and the time window (T) are the important design parameters for tuning the performance of the proposed VMM for a particular gate length of the MOSFET utilized in the 1T-1R block. The performance parameters of the VMM architecture for different input voltages (V_{GS}), time window (T), gate lengths (L_g), VMM sizes (M in $M \times M$ VMM) and non-linearity factor (β) of RRAM are listed in Table I. The output (worst case) error (e_{out}) was found by simulating multiple runs of VMM operation in HSPICE with different combination of random inputs and random weights in each run in an attempt to span the entire sample space of possible input and weight combinations. The line parasitics such as line resistances and capacitances and the corresponding process variations pertinent to the 55-nm technology node were also considered in the HSPICE simulations. The total energy dissipated in the load capacitor, E_{Cl} (which is the dominant energy dissipation mechanism as discussed later in section V) for the VMM operation has also been included in Table I. As can be observed from table I, the compute error is low and further reduces with increasing VMM size till $M < 100$. However, as the VMM size increases above 100, the line parasitics and their process variations lead to a non-negligible increase in the compute error. While the line resistances lead to a drop in the effective input (gate) voltage of the MOSFETs on the far end of the 1T-1R array leading to a reduced drain current, the line capacitances add to the latency. Although the differential configuration is effective in mitigating the impact of fixed line parasitics, the process variations cannot be compensated even exploiting a differential configuration and escalate the compute error.

From Table I, it can also be observed that there is a trade-off between the compute precision, dynamic range and the energy dissipated. For instance, to achieve a high compute precision of ~ 6 -bits for large sized VMMs ($M > 100$), a higher value of input voltage ($V_{GS} = 0.5$ V) should be used. A higher input voltage results in a higher maximum current (I_{max}) leading to a larger load capacitance. Although the dynamic range is also high for such operating conditions, the area and energy efficiency is limited by the load capacitor which dominates the area and energy landscape (as discussed in

TABLE I
DESIGN SPACE EXPLORATION

V_{GS} (V)	0.3 ($L_g = 120$ nm, $R_{ON} = 10K\Omega$, $R_{OFF} = 10M\Omega$)						0.3 ($L_g = 240$ nm, $R_{ON} = 10K\Omega$, $R_{OFF} = 10M\Omega$)						0.5 ($R_{ON} = 1M\Omega$)					
B	4			8			4			8			4 ($L_g = 120$ nm, $R_{OFF} = 9 M\Omega$)			4 ($L_g = 240$ nm, $R_{OFF} = 9.5 M\Omega$)		
$I_{max}; I_{min}$	136.9 nA ; 25.8 nA			137.5 nA ; 39.8 nA			125.9 nA ; 25.2 nA			126.3 nA ; 38.7 nA			497 nA ; 94.6 nA			496.5 nA ; 94.1 nA		
T (ns)	16	32	64	16	32	64	16	32	64	16	32	64	16	32	64	16	32	64
VMM size, $M = 10$																		
E_{Cl} (pJ)	0.09	0.19	0.39	0.09	0.19	0.39	0.09	0.18	0.36	0.09	0.18	0.36	0.3	0.7	1.4	0.3	0.7	1.4
$e_{out}, \%$	4.5	2.8	2.8	4.4	2.8	2.8	2.6	2.5	2.4	2.6	2.5	2.4	1.44	1.0	0.74	0.88	0.74	0.55
P_{out}	3	4	4	3	4	4	4	4	4	4	4	4	5	5	6	5	6	6
VMM size, $M = 50$																		
E_{Cl} (pJ)	2.45	4.92	9.85	2.47	4.95	9.9	2.25	4.53	9.06	2.27	4.5	9.09	8.93	17.8	36	8.95	17.8	36
$e_{out}, \%$	4.3	2.6	2.7	4.2	2.7	2.6	2.4	2.4	2.3	2.5	2.4	2.2	1.3	0.94	0.72	0.77	0.68	0.48
P_{out}	3	4	4	3	4	4	4	4	4	4	4	4	5	5	6	5	6	6
VMM size, $M = 100$																		
E_{Cl} (pJ)	9.81	19.7	39.4	9.9	19.8	39.6	9.0	18.1	36.2	9.09	18.2	36.3	35.7	71.5	144	35.6	71.4	144
$e_{out}, \%$	4.2	2.6	2.6	4.2	2.6	2.5	2.3	2.3	2.3	2.3	2.4	2.2	1.2	0.92	0.66	0.75	0.64	0.46
P_{out}	3	4	4	3	4	4	4	4	4	4	4	4	5	5	6	6	6	6
VMM size, $M = 200$																		
E_{Cl} (pJ)	39.2	78.4	157	39.6	79.2	158	36	72.5	145	36.3	72.7	145	142	286	576	142	285	576
$e_{out}, \%$	4.3	2.7	2.7	4.4	2.7	2.7	2.4	2.4	2.3	2.4	2.3	2.3	1.3	0.93	0.67	0.77	0.64	0.46
P_{out}	3	4	4	3	4	4	4	4	4	4	4	4	5	5	6	6	6	6

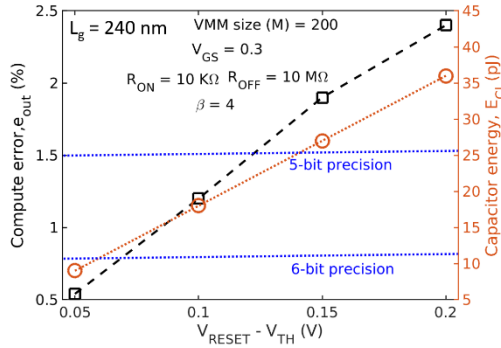


Fig. 5 Impact of variation in the threshold voltage of the neuron circuit (V_{TH}) to limit the maximum voltage swing across RRAM ($V_{RESET} - V_{TH}$) on the compute error and the capacitor energy of the proposed VMM approach.

Section V.

Moreover, to achieve a higher area and energy efficiency by limiting the size of the load capacitor, a lower input voltage may be used to reduce the maximum current (I_{max}). However, the compute precision and the dynamic range reduces significantly at such operating conditions. The weight precision may limit the compute precision in such cases.

Still, the preliminary results indicate that an effective compute precision of 6-bits is achievable for a VMM size, $M > 100$ using the proposed approach. In addition, depending on the targeted compute precision, input time window, VMM size, area, energy efficiency, voltage swing across RRAM etc. we may optimize the design parameters to achieve optimum performance of the proposed VMM architecture.

Since the conductance state of the RRAM is sensitive to the voltage drop across them, we have also analyzed the performance of the proposed VMM approach for neuron circuit with different threshold voltages ($V_{TH} > 0.5$ V) to limit the maximum voltage swing across RRAM ($V_{RESET} - V_{TH}$). As can be observed from Fig. 5, a reduction in the maximum voltage swing across RRAM leads to a higher compute precision owing to the lower CLM/DIBL error. Although a reduction in the

voltage drop across RRAM increases the load capacitor size according to equation (vii), the energy dissipated in the load capacitor, E_{Cl} decreases owing to the reduced voltage swing as shown in Fig. 5.

V. PERFORMANCE ESTIMATION

From Table I, it can be observed that the proposed VMM approach yields a compute precision of 3-bits to 6-bits depending on the design parameters. Targeting a compute precision of 4-bits, which is sufficient for several applications including neuromorphic computing [8], [10], we select an input voltage of 0.3 V, a time window of 16 ns and a gate length $L_g = 240$ nm for estimating the energy and area efficiency of the proposed approach. Fig. 6 shows the area and energy efficiency breakdown of the proposed VMM approach taking into account the input/output (I/O) peripheral circuitry and the neuron circuit for different VMM sizes.

The basic components of the VMM I/O circuitry are digital input to time-domain pulse converters (DTC) which consist of a 4-bit shared counter and a 4-bit digital comparator followed by a S-R latch for each input and time-domain pulse to digital output converters (TDC) which consist of a 4-bit accumulator for each neuron output. The 4-bit accumulator is realized using a 4-bit full adder and a 4-bit register based on D-flip flops. A shared clock enables conversion of the pulse duration of the neuron output to digital outputs. The neuron circuit consists of a S-R latch realized using a pair of NAND gates followed by an AND gate and NOT gate for implementing the differential scheme. The load capacitors are realized using MOSCAPs from the 55-nm technology node.

It can be observed from Fig. 6 that the I/O circuitry consumes a significant portion of the energy and area landscape of the proposed VMM architecture when the VMM size is small. However, the load capacitor (C_j) tends to dominate the area and energy landscape as the VMM size increases. The preliminary results indicate an effective compute precision of 4-bits with an energy efficiency of ~ 1.5 Pops/J and a

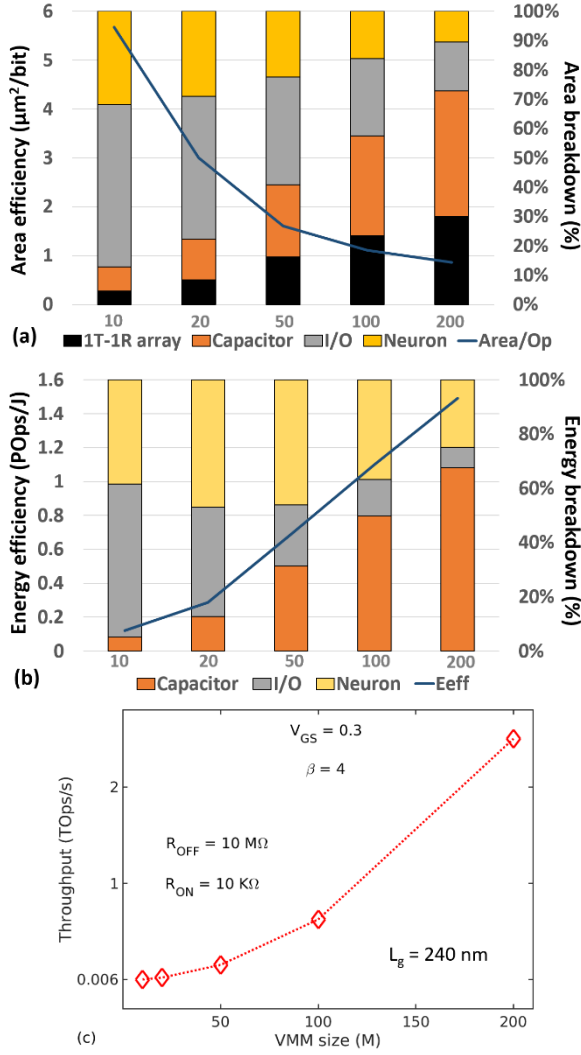


Fig. 6 The variation of (a) area efficiency, (b) energy efficiency and (c) throughput of the proposed VMM with VMM size (M) for a ReLU neuron.

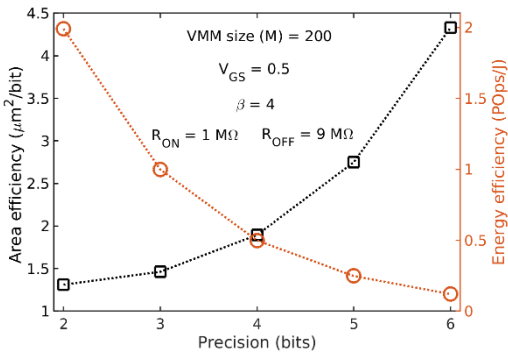


Fig. 7 The variation of area efficiency and energy efficiency of the proposed VMM with VMM size, $M = 200$ for different targeted precisions.

throughput of 2.5 Tops/s for VMM size = 200 utilizing the proposed approach.

Although applications such as inference, classification, recognition etc. may be performed with high accuracy utilizing even low precision (~ 4 bits) VMM operations [8], we also analyze the efficacy of the proposed approach for different target precisions higher than 4-bits with different operating

TABLE II
PERFORMANCE BENCHMARKING

Reference	[3]	[6]	[7]	[8]	[10]	[11]	[14]	This work
Approach	CM	CM	CM	SC	TD	TD	TD	TD
Process(nm)	180	22	180	40	14	250	55	55
Precision (bits)	3	~ 4	~ 5	3	< 8	~ 7	~ 6	6
EE(Tops/J)	6.4	60	5.7	8	18	< 290	80	498
I/O included	Yes	No	Yes	Yes	No	No	Yes	Yes
Results	Sim	Sim	Exp	Exp	Sim	Sim	Sim	Sim

CM: current-mode SC: switch-capacitor TD: time-domain

conditions as shown in Fig. 7. An increase in the targeted bit precision effectively increases the time window (T) to encode the inputs while operating at the same frequency. Therefore, the capacitor and I/O circuit area and energy consumption increases significantly with an increased target precision. This leads to a considerable degradation in the area and energy efficiency when targeting higher precision VMM operations as shown in Fig. 7. Moreover, we may utilize a lower conductance value for the ON-state of the RRAM to reduce I_{max} further and decrease load capacitance C_l for enhancing the energy and area efficiency while operating with a reduced precision (4-bits) as compared to the calculated compute precision (6-bits). Similarly, a lower reset voltage (V_{RESET}) may further increase the energy and area efficiency while enabling a compute precision of 4-bits. The capacitor area may also be reduced by using a different input encoding scheme whereby the individual input bits are encoded as discrete pulses and employing the switched capacitor scheme to reduce the charge integrated on the load capacitor [TBD].

Furthermore, the intrinsic thermal noise of the MOSFET and the random telegraph noise (RTN) in the RRAM may also affect the compute precision. Therefore, analysis of the proposed VMM approach under noise is an important future work.

VI. CONCLUSION

An energy-efficient time-domain VMM exploiting a modified configuration of 1T-1R array has been proposed in this work. The dominant mechanisms such as CLM, DIBL, etc. which degrade the performance of the proposed architecture are discussed in detail. Furthermore, we show that there exists a trade-off between the compute precision, dynamic range and the area and energy efficiency of the proposed VMM approach. Therefore, we also provide necessary design guidelines to further optimize the performance of the 1T-1R VMM. The preliminary results indicate an effective compute precision of 6-bits with a significantly high energy efficiency of ~ 498.5 TOPs/J as compared to the other proposed VMM approaches (Table II) and a throughput of 1.9 Tops/s for VMM size = 200 using the proposed approach. Our results may provide an incentive for experimental realization of the VMM approach based on 1T-1R array.

REFERENCES

- [1] Y. LeCun *et al*, "Deep learning," *Nature*, vol. 521, pp. 436-444, May 2015.
- [2] M. Mohammadi *et al*, "Deep Learning for IoT Big Data and Streaming Analytics: A Survey," in *IEEE Comm. Surv. Tut.*, vol. 20, no. 4, pp. 2923-2960, 2018.
- [3] J. Binas, D. Neil, G. Indiveri, S. C. Liu, and M. Pfeiffer, "Precise deep neural network computation on imprecise low-power analog hardware," *arXiv preprint arXiv:1606.07786*, 2016.

- [4] T. Tohara, H. Liang, H. Tanaka, M. Igarashi, S. Samukawa, K. Endo, Y. Takahashi and T. Morie, "Silicon nanodisk array with a fin field-effect transistor for time-domain weighted sum calculation toward massively parallel spiking neural networks," *Appl. Phys. Expr.*, vol. 9, no. 3, p.034201, 2016.
- [5] G. Burr *et al.*, "Experimental Demonstration and Tolerancing of a Large-Scale Neural Network (165,000 Synapses), using Phase-Change Memory as the Synaptic Weight Element," in *Proc. IEDM*, CA, Dec. 2014.
- [6] M. Hu *et al.*, "Dot-product engine for neuromorphic computing: programming 1T1M crossbar to accelerate matrix-vector multiplication," in *Proc. DAC*, Austin, TX, pp.1-6, 2016.
- [7] X. Guo, F. M. Bayat, M. Bavandpour, M. Klachko, M. R. Mahmoodi, M. Prezioso, K. K. Likharev, and D. B. Strukov, "Fast, energy-efficient, robust, and reproducible mixed-signal neuromorphic classifier based on embedded NOR flash memory technology," In *IEEE IEDM*, pp. 6-11, Dec 2017.
- [8] E. H. Lee, and S. S. Wong, "Analysis and design of a passive switched-capacitor matrix multiplier for approximate computing," *IEEE J. Solid-State Circuits*, vol. 52, no. 1, pp.261-271, 2017.
- [9] D. Miyashita, S. Kousai, T. Suzuki, and J. Deguchi, "A neuromorphic chip optimized for deep learning and cmos technology with time-domain analog and digital mixed-signal processing," *IEEE J. Solid-State Circuits*, vol. 52, no. 10, pp.2679-2689, 2017.
- [10] M. J. Marinella, S. Agarwal, A. Hsia, I. Richter, R. Jacobs-Gedrim, J. Niroula, S. J. Plimpton, E. Ipek, and C. D. James, "Multiscale co-design analysis of energy, latency, area, and accuracy of a ReRAM analog neural training accelerator," *IEEE J. Emerging and Selected Topics in Circuits and Systems*, vol. 8, no. 1, pp.86-101, 2018.
- [11] Q. Wang, H. Tamukoh, and T. Morie, "A Time-domain Analog Weighted-sum Calculation Model for Extremely Low Power VLSI Implementation of Multi-layer Neural Networks," *arXiv preprint arXiv:1810.06819*, 2018.
- [12] T. Morie, H. Liang, T. Tohara, H. Tanaka, M. Igarashi, S. Samukawa, K. Endo, and Y. Takahashi, "Spike-based time-domain weighted-sum calculation using nanodevices for low power operation," In *2016 IEEE-NANO*, pp. 390-392, 2016.
- [13] M. Yamaguchi, G. Iwamoto, H. Tamukoh, and T. Morie, "An Energy-efficient Time-domain Analog VLSI Neural Network Processor Based on a Pulse-width Modulation Approach," *arXiv preprint arXiv:1902.07707*. Feb 2019.
- [14] M. Bavandpour *et al.*, "Mixed-signal neuromorphic inference accelerators: Recent results and future prospects," in *Proc. IEDM'18*, San Francisco, CA, Dec. 2018.
- [15] M. Bavandpour *et al.*, "Energy-Efficient Time-Domain Vector-by-Matrix Multiplier for Neurocomputing and Beyond," *IEEE Trans. Circuits and Systems II*, 2019. doi:[10.1109/TCSII.2019.2891688M](https://doi.org/10.1109/TCSII.2019.2891688M).
- [16] B. Chakrabarti, M. A. Lastras-Montano, G. Adam, M. Prezioso, B. Hoskins, M. Payvand, A. Madhavan, A. Ghofrani, L. Theogarajan, K. T. Cheng, and D. B. Strukov, "A multiply-add engine with monolithically integrated 3D memristor crossbar/CMOS hybrid circuit," *Scientific rep.*, vol. 7, p.42429, 2017.
- [17] *HSPICE User Guide: Basic Simulation and Analysis*, Synopsys, Inc., 592 Mountain View, CA, USA, 2018.
- [18] B. Li *et al.* "RRAM-based analog approximate computing." *IEEE Trans. Computer-Aided Design of Integrated Circuits and Systems*, vol. 34, no. 12, pp. 1905-1917, 2015.
- [19] F. Alibart, *et al.* "High precision tuning of state for memristive devices by adaptable variation-tolerant algorithm." *Nanotechnology*, vol. 23, no. 7 2012.